JOURNAL OF GEOPHYSICAL RESEARCH, VOL. 97, NO. D18, PAGES 20,427–20,436, DECEMBER 20, 1992

The Effects of Sampling Frequency on the Climate Statistics of the European Centre for Medium-Range Weather Forecasts

THOMAS J. PHILLIPS AND W. LAWRENCE GATES

Program for Climate Model Diagnosis and Intercomparison, Lawrence Livermore National Laboratory, Livermore, California

KLAUS ARPE[1]

European Centre for Medium-Range Weather Forecasts (ECMWF), Reading, England

The effects of sampling frequency on the first- and second-moment statistics of selected European Centre for Medium-Range Weather Forecasts (ECMWF) model variables are investigated in a simulation of "perpetual July" with a diurnal cycle included and with surface and atmospheric fields saved at hourly intervals. The shortest characteristic time scales (as determined by the e-folding time of lagged autocorrelation functions) are those of ground heat fluxes and temperatures, precipitation and runoff, convective processes, cloud properties, and atmospheric vertical motion, while the longest time scales are exhibited by soil temperature and moisture, surface pressure, and atmospheric specific humidity, temperature, and wind. The time scales of surface heat and momentum fluxes and of convective processes are substantially shorter over land than over oceans. An appropriate sampling frequency for each model variable is obtained by comparing the estimates of first- and second-moment statistics determined at intervals ranging from 2 to 24 hours with the "best" estimates obtained from hourly sampling. Relatively accurate estimation of first- and second-moment climate statistics (10% errors in means, 20% errors in variances) can be achieved by sampling a model variable at intervals that usually are longer than the bandwidth of its time series but that often are shorter than its characteristic time scale. For the surface variables, sampling at intervals that are nonintegral divisors of a 24-hour day yields relatively more accurate time-mean statistics because of a reduction in errors associated with aliasing of the diurnal cycle and higher-frequency harmonics. The superior estimates of first-moment statistics are accompanied by inferior estimates of the variance of the daily means due to the presence of systematic biases, but these probably can be avoided by defining a different measure of low-frequency variability. Estimates of the intradiurnal variance of accumulated precipitation and surface runoff also are strongly impacted by the length of the storage interval. In light of these results, several alternative strategies for storage of the EMWF model variables are recommended.

1. INTRODUCTION

While studies of the effects of spatial resolution on climate model simulations span the last two decades [e.g., *Manabe et al.*, 1970; *Wellck et al.*, 1971; *Boer and Lazare*, 1988; *Boville*, 1991; *Kiehl and Williamson*, 1991], the impact of temporal resolution has only recently received much attention [e.g., *Phillips*, 1987; *Kidson and Trenberth*, 1988; *Thuburn*, 1991]. Sampling frequency is an important consideration for climate studies, since geophysical variables fluctuate over a wide range of time scales. The sampling problem is made more difficult by the typical computer storage procedure for general circulation models (GCMs): while many variables are updated at every time step, the simulation history usually is saved at much coarser intervals. In effect, "snapshots" of the instantaneous climate state are obtained only a few times and at the same times each day. Such a procedure may be an unavoidable consequence of storage constraints, but its impact on model climate statistics needs to be better understood. Moreover, sampling frequency is an especially important issue for the majority of present-day general circulation models that simulate the diurnal cycle [e.g., *Hansen et al.*, 1983; *Boer et al.*, 1984; *Tokioka et al.*, 1984; *Slingo*, 1985] since the climate statistics may be impacted by errors associated with the aliasing of the diurnal cycle and higher harmonics [*Thuburn*, 1991; *Trenberth*, 1991].

We investigate this sampling problem by analyzing selected variables from a numerical experiment with the European Centre for Medium-Range Weather Forecasts (ECMWF) atmospheric model. The model and the experimental design are described in more detail in section 2.

Three interrelated questions are considered.

1. What are minimum acceptable sampling frequencies for accurate estimation of the climate statistics of different model variables?
2. What are the relationships between these sampling frequencies and the characteristic time scales and structures of variability of the model climate?
3. How are the climate statistics of the model variables impacted by sampling at the same times versus different times each day?

We address the first two questions by comparing climate statistics derived from hourly sampling with those obtained from sampling at coarser intervals and by computing other statistical measures of time scale and variability. We investigate the third question by comparing the climate statistics determined from sampling at intervals that divide evenly into a 24-hour day versus those intervals that do not. We describe

[1]Now at Max-Planck-Institut für Meteorologie, Hamburg, Germany.

Paper number 92JD02020.
0148-0227/92/92JD-02020$05.00

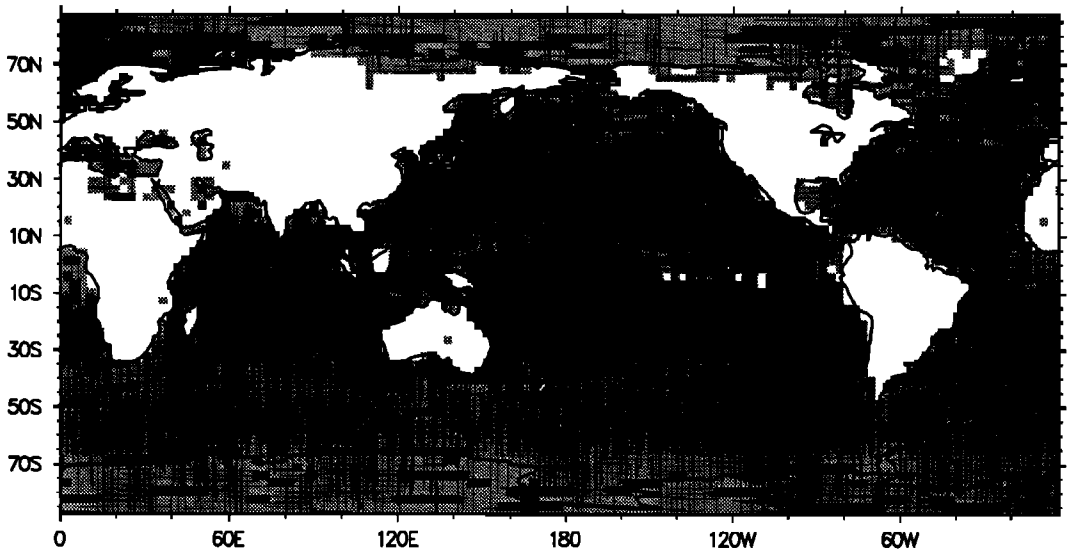

Fig. 1. Map of e-folding time τ (rounded to nearest hour) of the lagged autocorrelation function of surface latent heat flux in a perpetual July integration of the ECMWF atmospheric general circulation model. Values less than 6 hours are unshaded, values between 6 and 20 hours are lightly shaded, and values greater than 20 hours are darkly shaded.

our methodology and results in section 3 and state our conclusions in section 4.

2. Model Description and Experimental Design

In this study we used cycle 33 of the ECMWF GCM, with 19 vertical levels and spectral T42 horizontal resolution. The model's global primitive equation dynamics [*ECMWF Research Department*, 1988*a*] are complemented by extensive parameterizations of atmospheric and surface physics. Cycle 33 differs from its model predecessor [*ECMWF Research Department*, 1988*b*] in the parameterizations of radiation [*Morcrette*, 1989], convection [*Tiedtke*, 1989], and gravity wave drag [*Miller et al.*, 1989].

We integrated the model for a total of 60 days with the solar declination fixed in perpetual July mode but with a diurnal cycle included. July climatological sea surface temperatures and sea ice limits were prescribed [*Alexander and Mobley*, 1976], but soil temperature, moisture, and runoff were allowed to vary in "surface" and "deep" layers at approximately 0.1- and 0.4-m depths, respectively (cf. *ECMWF Research Department* [1988*b*] for parameterization details). The model atmosphere was initialized from an operational ECMWF data set for June 1, 1986. Model spin-up, as determined from the equilibration of global-integral energetics, was achieved within the first 10 days of the simulation. We analyzed the remaining 50 days of the integration.

The simulation of July climate was motivated by a desire to investigate variables related to convection and to land surface processes that are especially vigorous in northern summer. The perpetual mode, while less realistic than a seasonal cycle integration, produced a quasi-stationary time series which rendered statistical analysis of the experiment more straightforward. In a departure from the standard procedure for the model, at every hour of the integration, radiative fluxes were calculated and accumulations of precipitation and surface runoff were reset to zero. Hourly snapshots of more than two dozen selected variables (cf. Table 1) were saved.

3. Methodology and Results

3.1. *Characteristic Time Scales of Model Variables*

Information on the characteristic time scale of a model variable V is provided by its lagged autocorrelation function A, calculated at each Gaussian grid point (i, j) from

$$A(i, j, k) = \sum_t [V(i, j, t) - \mu(i, j)] \cdot [V(i, j, t + k) - \mu(i, j)]/(N\sigma^2)$$

where t is the time history and k is the lag in 1-hour increments, N is the number of hourly time samples, μ is the time mean of variable V, and σ^2 is its time variance.

For increasing lag $k > 0$, $A(i, j, k)$ decreases below its zero-lag value of unity. Often, this decrease is monotonic, but relative increases also can occur at lags related to dominant frequencies in the time series of the variable. The field of e-folding time $\tau(i, j)$, defined as the minimum lag k such that

$$A(i, j, k) \leq e^{-1} \approx 0.368$$

is a measure of characteristic time scale.

The geographical distribution $\tau(i, j)$ was computed for each variable. An example is shown for the surface latent heat flux in Figure 1. The details of this field are complex, but a clear geographical contrast is apparent: except for Antarctica where there is only a weak diurnal cycle, the e-folding times over the continents are substantially shorter than over most of the ocean and sea ice regions. Because the values of a number of other model variables showed a sensitivity to surface type, we calculated an area-weighted land average τ_L in addition to the area-weighted global average τ_G, which is strongly influenced by the e-folding

TABLE 1. Area-Weighted Land/Global (L/G) Averages, Rounded to the Nearest Hour, of Sampling Statistics of Selected Model Variables

	Variable				
	τ_L/τ_G	S_L/S_G	s_{95L}/s_{95G}	s_{99L}/s_{99G}	P_L/P_G
Surface dn SW flux*	4/4	3/3	6/6	3/3	5/5
Surface up SW flux*	4/4	3/3	6/6	3/3	5/5
Convective mass flux*	4/9	3/5	2/2	1/1	23/40
Convective precipitation†	5/10	3/5	2/3	1/1	37/41
Surface sensible heat flux*	5/18	3/6	4/9	2/4	13/55
Surface latent heat flux*	5/21	2/4	3/7	2/2	16/58
Convective cloud cover‡	6/12	3/5	2/2	1/1	34/45
Surface soil runoff†	7/···	3/···	2/···	1/···	45/···
Convective cloud top‡	7/10	8/11	2/2	1/1	32/35
Convective cloud base‡	8/11	8/12	2/2	1/1	33/38
MT vertical velocity‡	8/9	8/9	5/5	4/4	41/45
Surface soil temperature*	9/···	5/···	9/···	5/···	26/···
Surface up LW flux*	9/19	5/8	9/11	5/7	26/56
Total cloud cover‡	11/13	8/9	4/5	2/2	49/54
Cloud liquid water‡	12/17	8/10	4/6	2/2	50/59
Vegetation canopy moisture*	13/···	6/···	7/···	3/3	62/···
Outgoing LW flux‡	13/16	10/11	5/5	2/2	52/58
Surface v stress*	18/23	11/12	9/12	4/6	62/72
Surface u stress*	19/27	11/12	9/12	4/6	60/74
MT v wind‡	27/24	12/12	14/14	8/8	78/77
MT specific humidity‡	27/27	24/24	15/17	8/9	77/78
Surface pressure*	36/36	10/10	17/19	9/9	77/80
MT u wind‡	46/46	24/24	17/18	8/9	87/87
MT temperature‡	47/42	24/24	17/17	8/8	85/85
Deep soil temperature*	49/···	12/···	21/···	11/···	81/···
Surface soil moisture*	59/···	12/···	27/···	9/···	95/···
Deep soil moisture*	91/···	24/···	48/···	14/···	99/···

Statistics include area-averaged values of e-folding time τ of the lagged autocorrelation function, maximum acceptable sampling interval S (cf. section 3.8), bandwidth intervals s_{95} and s_{99} (cf. section 3.9), and the percentage p of the total variance that is explained by the variance of the daily means. "Midtropospheric" (MT) level is approximately 500 hPa for a surface pressure of 1000 hPa; "surface soil" and "deep soil" denote layers at depths of about 0.1 and 0.4 m, respectively. SW, shortwave; LW, longwave; dn, downward; up, upward.

*Denotes a (category 2) variable whose first-moment statistics are closer to the best estimate at sampling intervals that are nonintegral divisors (NID) of a 24-hour day than are those of neighboring sampling intervals.

†Indicates that the variable is accumulated over time.

‡Denotes a (category 1) variable whose first-moment statistics grow steadily farther from the best estimate (obtained by hourly sampling) with increasing sampling interval.

times over the more extensive ocean and sea ice surfaces. The area average e-folding times of the selected climate variables are listed in the order of the τ_L value in Table 1. The time scales of surface longwave, sensible, and latent heat fluxes and of convective mass flux, cloud cover, and precipitation are substantially shorter over land than over the oceans and sea ice, as evidenced by the sizeable differences in τ_L and τ_G. A similar pattern is displayed by the surface wind stresses, a result of the larger surface roughness of the continents.

From Table 1 the shortest time scales (τ_L = 4–12 hours) are associated with surface heat fluxes, soil temperature and runoff, convective processes, cloud amount and liquid water content, and atmospheric vertical motion. The longest time scales (τ_L > 24 hours) are exhibited by surface pressure, atmospheric specific humidity, temperature and wind, deep soil temperature, and surface and deep soil moisture. Vegetation canopy moisture, outgoing longwave radiation, and surface wind stress have intermediate values of τ_L in the range 13–24 hours.

The characteristic time scales of zonal and meridional wind, vertical motion, specific humidity, and temperature are listed only at midtropospheric (MT) levels in Table 1. The vertical profiles of global average τ values of these variables are shown in Figures 2a and 2b. The time scales of temperature and zonal wind (Figure 2a) are longer in the free atmosphere than in the boundary layer, while e-folding times for specific humidity and vertical motion are largest near the surface (Figure 2b). (The time scale of the meridional wind is relatively invariant with altitude.) The temperature field fluctuates less at higher levels because diurnal variations in heat fluxes are larger in the boundary layer, and the u wind is steadier at high altitudes where persistent jet streams dominate. In contrast, orography forces a strong steady component in the near-surface vertical motion field. Specific humidity may follow a pattern similar to that of vertical motion because moister air correlates with rising motion and drier air with sinking motion.

3.2. *First- and Second-Moment Climate Statistics*

For a system as complex as a GCM the τ value can provide only a rough indication of an appropriate sampling interval for a model variable. It is therefore necessary to determine

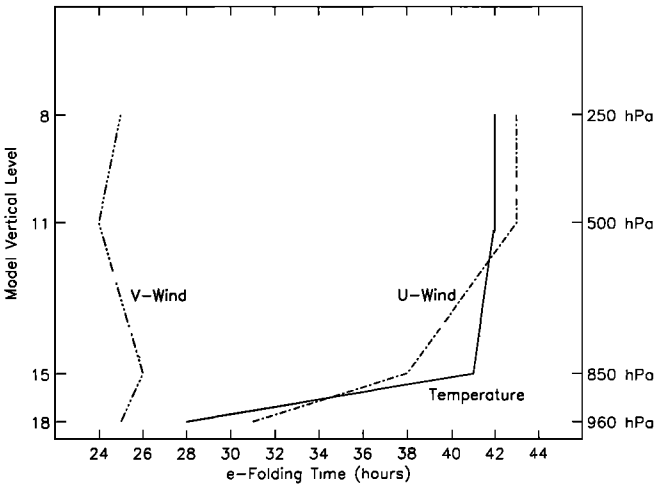

Fig. 2*a*. Vertical profiles of global average *e*-folding times τ (rounded to the nearest hour) of atmospheric temperature, u wind, and v wind. The profiles include data points at model vertical levels 8, 11, 15, and 18 which, for a surface pressure of 1000 hPa, correspond approximately to 250, 500, 850, and 960 hPa pressure levels.

more explicitly the impact of sampling frequency on the climate statistics of the model. The focus in this study was on first- and second-moment statistics of different types. That is, using all the hourly samples of the field $V(i, j)$ of each variable we calculated the best estimate $\mu(i, j, s)$, s = 1 hour, of the time mean as well as the means $\mu(i, j, s)$ corresponding to sampling intervals $s = 2, 3, \cdots, 12$, and 24 hours (by taking every other sample to compute the time mean for interval $s = 2$, every third sample for interval s = 3, etc.).

We also calculated the daily mean of each day d as a function of interval s from

$$\mu_d(i, j, s) = \sum_{t}^{N_d(s)} V(i, j, ts)/N_d(s)$$

where $N_d(s)$ is the number of samples of $V(i, j)$ available on day d for sampling interval s. Note that when s divides evenly into a 24-hour day, the variable is sampled at the same times each day and the number of daily samples N_d is constant; however, when s is a nonintegral divisor (NID) of 24 hours (i.e., s = 5, 7, 9, 10, or 11 hours), V is sampled at different times each day, and N_d varies. For example, if s = 5 hours, N_d is usually 5, but every fifth day it is 4. Thus the daily means of fields exhibiting a strong diurnal cycle will show a spurious variation associated with this sampling bias.

In addition, we computed two types of second-moment statistics for each field: the total variance σ_T^2 that includes the intradiurnal fluctuations about the mean and the variance σ_D^2 of the daily means about the 50-day mean that is defined by

$$\sigma_D^2(i, j, s) = \sum_{d=1}^{N_D} [\mu_d(i, j, s) - \mu(i, j, s)]^2/(N_D - 1)$$

where N_D = 50 is the number of daily means in the record.

The variance σ_D^2 includes only the contributions from fluctuations of lower frequency than 1 day^{-1}, and so $\sigma_D^2/\sigma_T^2 \leq 1$, with the fractional value being a function of model variable and location. For many climate studies, however, σ_D^2 is of greater interest than σ_T^2.

The best estimate (from hourly samples) of the area-weighted global percentage

$$p_G = (\sigma_D^2/\sigma_T^2)_G \times 100$$

and the land average value p_L are listed for each model variable in Table 1. It can be seen that the model's deep soil temperature, soil and vegetation canopy moisture, surface pressure and wind stress, and atmospheric specific humidity, temperature, and wind mostly vary at lower frequencies, while there is large intradiurnal variability in the surface heat fluxes and soil temperature, convective processes, precipitation and runoff, and vertical motion. The variance of total cloud cover and liquid water content, and of outgoing longwave radiation is almost evenly divided between intradiurnal and lower-frequency fluctuations.

As expected, shorter *e*-folding times τ in Table 1 are mostly associated with fields that exhibit large variability at intradiurnal frequencies (i.e., lower p values). Surface longwave, sensible, and latent heat fluxes and atmospheric convective processes also show differences between land average variance percentages p_L and global averages p_G that are similar to their τ_L-τ_G differences.

3.3. *Statistical Measures of Sampling Frequency Effects*

In determining the impact of sampling frequency on first- and second-moment climate statistics, we sought appropriate measures of the departures of $\mu(i, j, s)$, $\sigma_T^2(i, j, s)$, and $\sigma_D^2(i, j, s)$, $s = 2, 3, \cdots, 12$, and 24 hours, from the best estimates $\mu(i, j, 1)$, $\sigma_T^2(i, j, 1)$, and $\sigma_D^2(i, j, 1)$. While t and F statistics are commonly used for testing the significance of differences in means and variances [*Fisher*, 1925], the element of statistical independence necessary for applying these tests was absent in this study because the samples were drawn from the same population. Nevertheless, suitably modified t and F statistics defined by

$$t_T(i, j, s) = |\mu(i, j, s) - \mu(i, j, 1)|/\sigma_T(i, j, 1)$$

$$t_D(i, j, s) = |\mu(i, j, s) - \mu(i, j, 1)|/\sigma_D(i, j, 1)$$

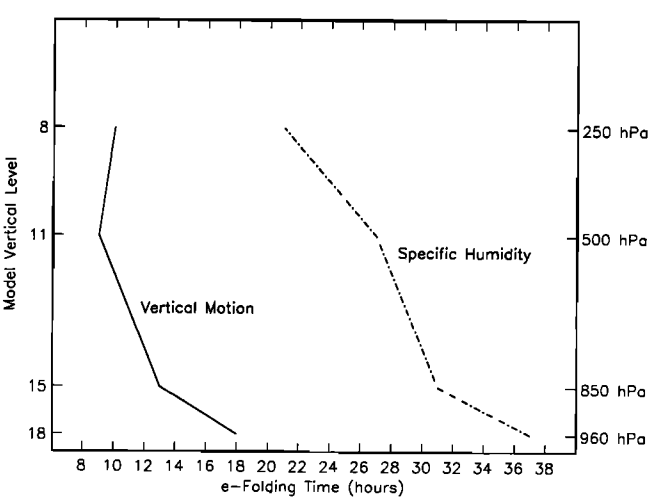

Fig. 2*b*. As in Figure 2*a*, except for atmospheric vertical motion and specific humidity.

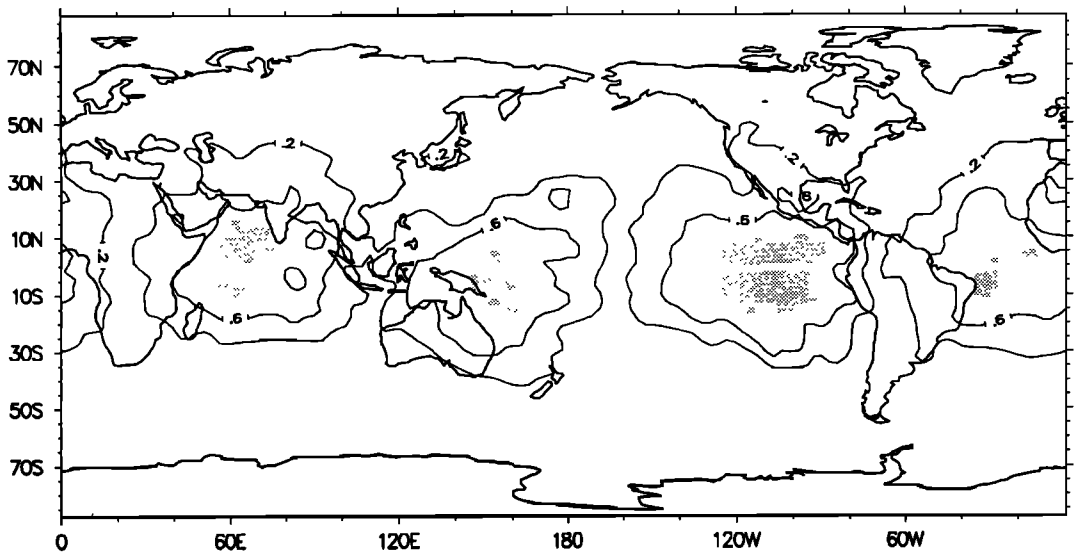

Fig. 3*a*. Field of first-moment statistic t_T of surface pressure for a sampling interval of 12 hours. Contours are at 0.2 and 0.6, with values greater than 1.0 shaded.

$$F_T(i, j, s) = \sigma_T^2(i, j, s)/\sigma_T^2(i, j, 1)$$

$$F_D(i, j, s) = \sigma_D^2(i, j, s)/\sigma_D^2(i, j, 1)$$

served as useful measures of the errors in estimating the means and variances for sampling intervals $s = 2, 3, \cdots, 12$, and 24 hours relative to the best estimates obtained from hourly sampling. These differed from "standard" t and F statistics in that there was no dependence on degrees of freedom and the divisors were not pooled combinations of $\sigma(i, j, 1)$ and $\sigma(i, j, s)$; rather, these measures were defined to allow the impact of sampling frequency on the climate statistics of different variables to be readily compared. Area-weighted global averages t_T, t_D, F_T, and F_D were computed to assist such a comparison.

We found that the t and F statistics for the model's surface variables show a qualitatively greater sensitivity to sampling frequency than do those of the atmospheric variables. For example, the errors in estimating the time mean of surface pressure for a sampling interval of 12 hours are indicated by the field of the t_T statistic in Figure 3*a*.

The largest errors occur in the tropics and are of the order of the standard deviation σ_T (i.e., $t_T \cong 1$). The pattern of the errors is that of the semidiurnal atmospheric tide, which is aliased into the time mean of the surface pressure field at a sampling interval of 12 hours [*Thuburn*, 1991; *Trenberth*, 1991]. Large aliasing errors also are apparent in the estimates of the total variance σ_T^2 of surface pressure at a 12-hour sampling interval, as evidenced by the field of F_T (Figure 3*b*). In the tropics the variance is underestimated by more than 60% ($F_T < 0.4$), while in some

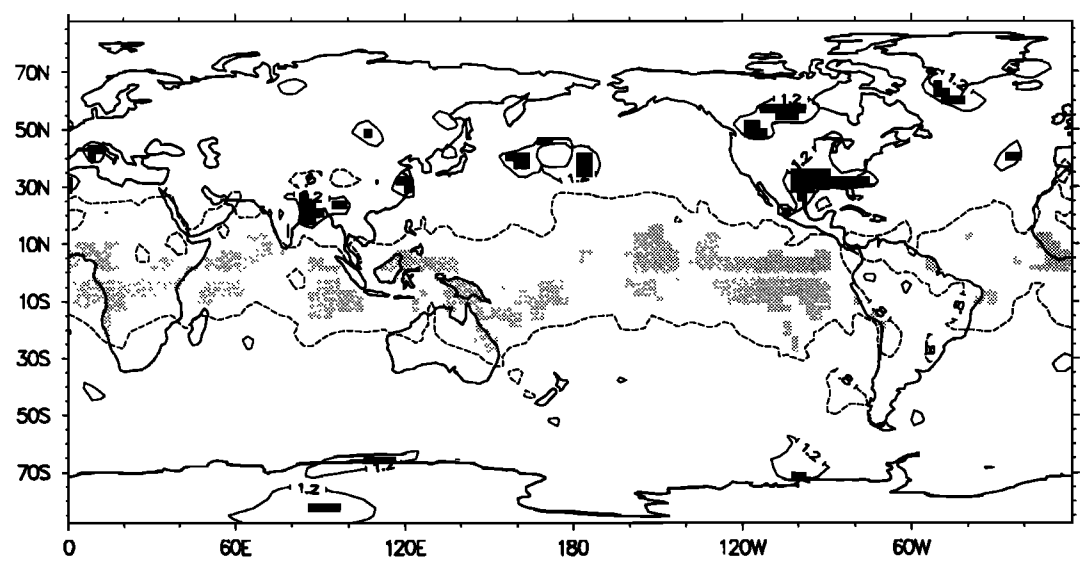

Fig. 3*b*. Field of second-moment statistic F_T of surface pressure for a sampling interval of 12 hours. Underestimation of variance by 20% ($F_T = 0.8$) is indicated by the dashed-line contour, with F_T values less than 0.4 lightly shaded. Overestimation of variance by 20% ($F_T = 1.2$) is indicated by the solid contour, with F_T values greater than 1.3 darkly shaded.

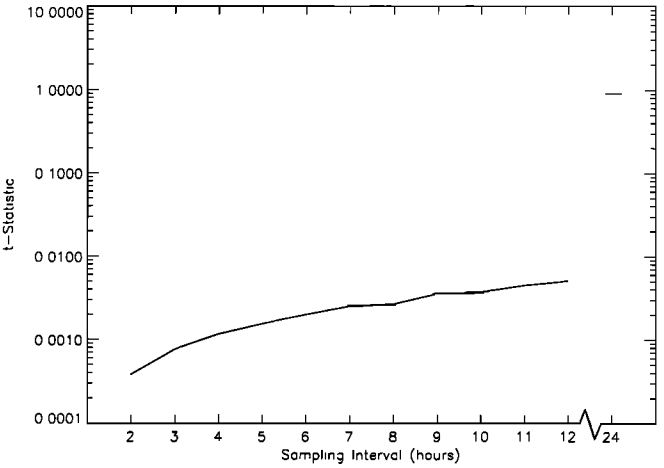

Fig. 4*a*. Average t_T statistic as a function of sampling interval for an ensemble of 120 time series, each consisting of 50 constant amplitude sine waves with a 24-hour period but with phase differing by 3° increments. Note the logarithmic scale on the ordinate. Also note here and in following figures the break in the abscissa and the absence of data between $s = 12$ hours and $s = 24$ hours.

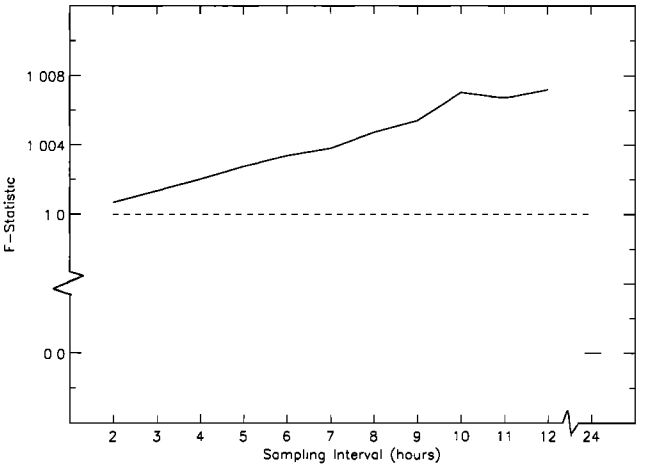

Fig. 4*b*. As in Figure 4*a*, except for the F_T statistic. The optimal value $F_T = 1.0$ is shown by the dashed line. Note the different ordinate scale below and above 1.0.

mid-latitude regions it is overestimated by more than 30% ($F_T > 1.3$).

On the other hand, the estimation errors in the climate statistics of most of the atmospheric variables do not become substantial until the sampling interval increases to 24 hours, when the diurnal cycle is aliased into the climate statistics. Even then, large errors are usually confined to small regions.

3.4. *Statistical Measures for an Idealized Case*

As a benchmark for the analysis that is to follow, it is instructive to consider a train of 50 constant amplitude sine waves, each with a 24-hour period (a highly idealized representation of the local diurnal cycle of a model variable for the 50-day integration). In this special case the variance σ_D^2 is zero (because the daily means μ_d are the same), and so the relevant statistics are $t_T(s)$ and $F_T(s)$. Because their values also depend on the phase of the wave train, we calculated $t_T(s)$ and $F_T(s)$ for 120 values of phase differing by 3° increments and then averaged over this ensemble. This procedure is equivalent to calculating $t_T(s)$ and $F_T(s)$ for an idealized diurnal cycle on grid points spaced every 3° longitude (the approximate equivalent grid spacing of the spectral T42 model) and then averaging around the latitude circle.

The ensemble average values t_T and F_T are plotted as a function of sampling interval s in Figures 4*a* and 4*b*, respectively. The t_T statistic grows fairly smoothly with sampling interval up to $s = 12$ hours, where the errors in estimating the time mean are still less than 1% of the standard deviation σ_T (Figure 4*a*). However, at $s = 24$ hours, the estimation error sharply increases as a result of the aliasing of the diurnal cycle into the time mean when sampling occurs only once per day. From Figure 4*b* it is seen that at all sampling intervals $2 \leq s \leq 12$ hours, the total variance is overestimated ($F_T > 1$) but by less than 1%. In this range the errors grow almost linearly with sampling interval. At $s = 24$ hours, however, the variance is grossly underestimated ($F_T = 0$) (another consequence of the aliasing of a constant amplitude diurnal cycle).

3.5. *Sampling Frequency and First-Moment Climate Statistics*

We found that the relationship of both t_T and t_D to sampling interval is qualitatively similar and falls into two categories for the ECMWF model variables (designated by the double dagger and asterisk in Table 1). The 11 category 1 variables (Figure 5) are all atmospheric fields with area average t statistics that increase smoothly with sampling interval in a way similar to the idealized case of Figure 4*a*. By contrast, the 14 variables in the second category (Figure 6) are mostly surface fields whose first-moment statistics are estimated more accurately by sampling at intervals that are NIDs of a 24-hour day (e.g., at $s = 5$, 7, 9, 10, or 11 hours) than at neighboring even-valued sampling intervals. However, at a given sampling interval the t-statistics of the category 1 variables (Figure 5) are several times smaller than

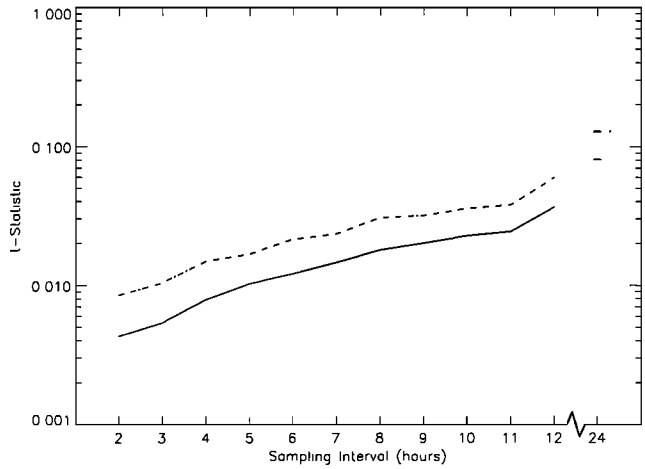

Fig. 5. Cross-variable average of area-weighted global t_T statistic (solid curve) and average plus cross-variable standard deviation (dotted-dashed curve) as a function of sampling interval for the category 1 (atmospheric) variables of Table 1. The optimal value of t_T is zero. Note the logarithmic scale on the ordinate. In this and in the following figures at $s = 24$ hours the cross-variable average is designated by a dash and the cross-variable scatter by a dash and dot.

those of the category 2 variables (Figure 6), implying that for the same sampling frequency the time means of the atmospheric fields can be estimated with considerably greater accuracy.

The error in estimating the first-moment statistics due to aliasing of the diurnal cycle is apparent. Estimation error also increases noticeably at $s = 12$ hours as a result of the aliasing of the semidiurnal cycle. Hence if snapshots from a long simulation can only be saved twice per day, it is preferable to store the variables at 11-hour rather than 12-hour intervals. The increase in aliasing error at $s = 12$ hours is much more abrupt for the surface variables (Figure 6) because the semidiurnal harmonic is a greater part of the intradiurnal variability of these fields. It follows that the larger errors in the time means of the surface variables at even-numbered sampling intervals relative to neighboring NID intervals result from the aliasing of still higher-frequency harmonics that contribute part of the intradiurnal variability of these fields. Another perspective is that the relative decrease in estimation error at the NID intervals is a result of more comprehensive sampling of the surface fields, since at these frequencies, sampling is done at different times each day.

3.6. *Sampling Frequency and Second-Moment Climate Statistics*

The aggregated F_T statistic for the atmospheric fields (not shown) remains between values of 1.0 and 1.01, indicating that total variance σ_T^2 is only slightly overestimated at all sampling frequencies. Estimation of the total variance of the surface fields (not shown) is accurate to within 3% at sampling intervals up to 12 hours, but at $s = 24$ hours, the variance is underestimated by about 20% on average.

The different impact of sampling frequency on the second-moment statistics of the atmospheric variables versus those for the surface variables is more dramatically revealed in the global average F_D statistics. The error in estimating the variance σ_D^2 of the daily means of the atmospheric variables about their 50-day means (Figure 7) increases linearly with sampling interval up to $s = 12$ hours, but due to aliasing of the diurnal cycle the average error in estimating σ_D^2 is more than 60% ($F_D > 1.6$) at $s = 24$ hours. The variance σ_D^2 of

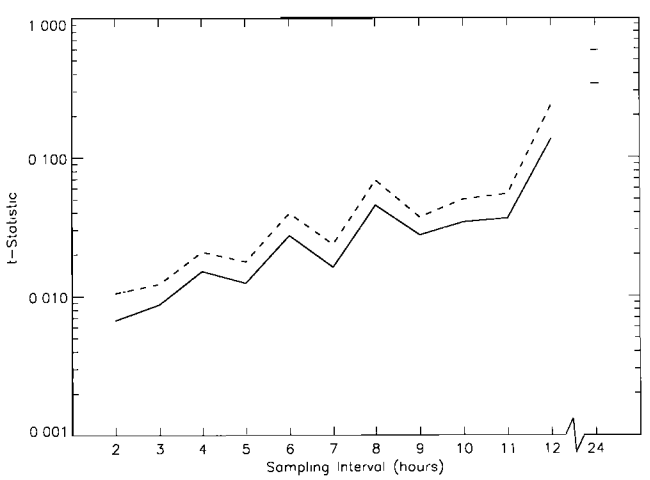

Fig. 6. As in Figure 5, except for the category 2 (mostly surface) variables of Table 1.

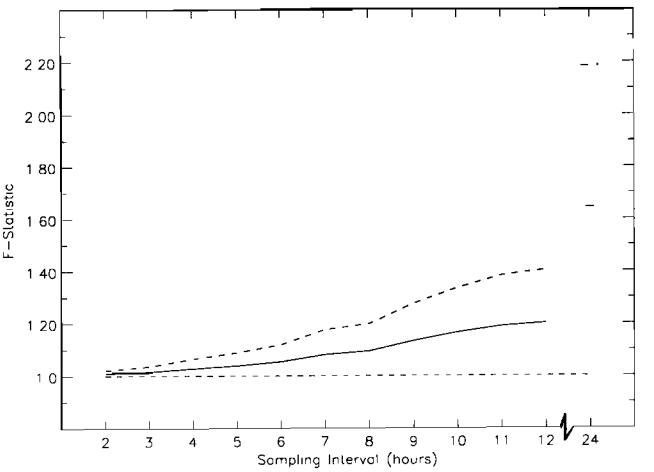

Fig. 7. Cross-variable average of area-weighted global F_D statistic (solid curve) and average cross-variable standard deviation (dotted-dashed curve) as a function of sampling interval for the category 1 (atmospheric) variables of Table 1. The optimal value $F_D = 1.00$ is also shown for comparison (dashed line).

daily means of the surface fields shows a qualitatively different dependence on sampling frequency, with large estimation errors evident at the NID intervals (Figure 8*a*). These errors are due to systematic biases in estimating the daily means μ_d brought about because sampling at the NID intervals is done at different times each day and the number of daily samples varies. Biases therefore also result in the variance σ_D^2 of the daily means μ_d which increase with NID sampling interval as the number of daily samples decreases. The largest errors are associated with the surface shortwave fluxes because they are especially sensitive to the time of day when sampling takes place, but sizeable errors remain at NID sampling intervals $s = 9$, 10, and 11 hours for the surface heat fluxes, convective mass flux, shallow soil temperature, and surface pressure (Figure 8*b*).

These sampling biases probably could be greatly reduced by estimating low-frequency variance from means obtained over periods containing a fixed number of samples, e.g., by calculating 5-day means for a sampling interval $s = 5$ hours, etc. Because most of the atmospheric fields do not exhibit as much intradiurnal variability as the surface fields (cf. Table 1), σ_D^2 can be estimated with acceptable accuracy at the NID sampling frequencies (Figure 7).

3.7. *Sampling Frequency and Accumulated Quantities*

Instead of saving snapshots of model variables, their values can be accumulated at each time step and stored at intervals s'. In principle, this procedure allows first-moment statistics to be determined "exactly" (to within numerical roundoff); similarly, accumulating squared values permits exact determination of second-moment statistics. In practice, however, storing accumulations instead of snapshots precludes the possibility of accurately determining the statistics of additional derived quantities. For example, the time series of quadratic quantities such as momentum and heat fluxes are systematically underestimated when derived a posteriori from accumulations of the state variables [*Thuburn*, 1991]. Thus unless all the quantities of interest can be identified a priori and computed efficiently at each time

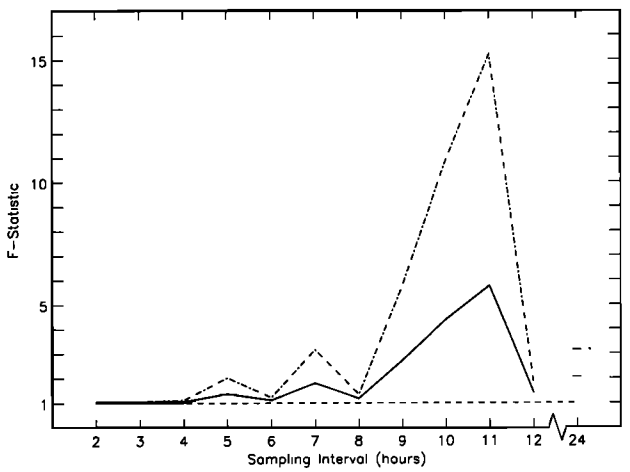

Fig. 8*a*. As in Figure 7, except for the category 2 (mostly surface) variables of Table 1.

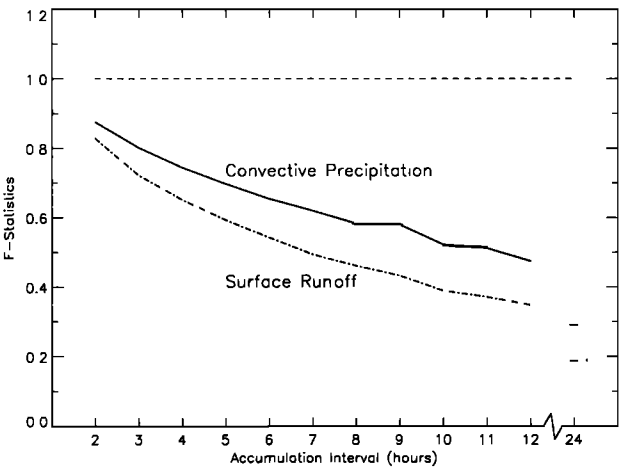

Fig. 9. Area-weighted global F_T statistic for accumulations of convective precipitation and surface soil runoff as a function of accumulation storage interval s'. Dashed-dotted curve indicates optimal value.

step, a strategy of saving accumulations instead of snapshots is problematical.

For the ECMWF model, however, it is common practice to selectively store accumulations of rapidly fluctuating variables such as precipitation and runoff, usually at 24-hour intervals. In this case the first-moment statistics as well as the variance of the daily means are known exactly, but the part of the total variance σ_T^2 that is due to intradiurnal fluctuations is indeterminate. In the present study, however, accumulations of precipitation and runoff were stored at hourly intervals, making it possible to estimate the total variance $\sigma_T^2(i, j, s')$ for different storage intervals $s' \geq 1$. Analogous to the treatment of the other model fields, the sensitivity of the variance of the accumulated variables to storage interval s' was measured by the statistic

$$F_T(i, j, s') = \sigma_T^2(i, j, s')/\sigma_T^2(i, j, 1)$$

Global averages $F_T(s')$ are shown for accumulated convective precipitation and surface soil runoff in Figure 9. At all storage intervals the variance $\sigma_T^2(s')$ of both variables is underestimated ($F_T < 1$) relative to $\sigma_T^2(1)$ and estimates of second-moment statistics degrade rapidly with increasing s'.

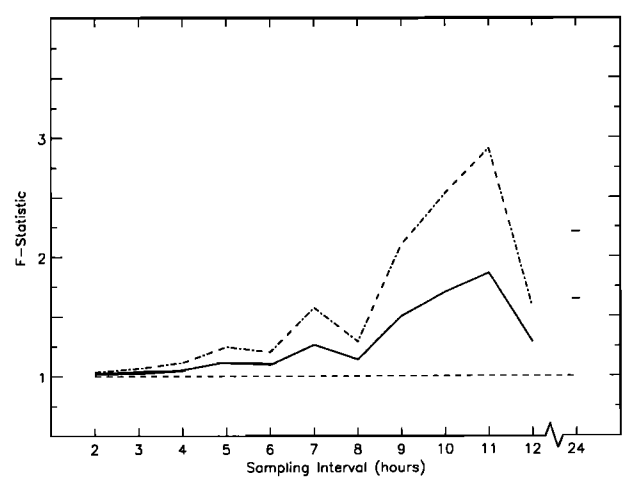

Fig. 8*b*. As in Figure 8*a*, but excluding the F_D statistics for surface upward and downward shortwave radiative fluxes.

Since a large part of the variance of accumulated precipitation and runoff is at intradiurnal frequencies (Table 1), such inaccurate estimation of σ_T^2 may be of concern for some climate applications.

3.8. *Maximum Acceptable Sampling Intervals*

The substantial cross-variable scatter in the t and F statistics of Figures 5–8 is an indication of the wide range of sensitivity to sampling frequency displayed by different model variables. From knowledge of these sampling effects, a maximum acceptable sampling interval S can be determined as

$$S = \max s \text{ such that } t_D(s) \leq b \text{ and } B^{-1} \leq F_D(s) \leq B$$

where b and B are specified error bounds. Here t_D and F_D are used as measures of estimation errors since they are usually the more relevant statistics for climate studies. Because only the intradiurnal variance of accumulated quantities is impacted by the storage interval s', a maximum acceptable accumulation interval S' is specified as

$$S' = \max s' \text{ such that } C^{-1} \leq F_T(s') \leq C$$

Prescribing $b = 0.1$, $B = 1.2$, and $C = 1.5$ as tolerable error bounds, the corresponding area-weighted sampling (or accumulation storage) intervals are listed in Table 1. As is to be expected, the shortest values of S are usually associated with relatively large values of intradiurnal variability. For many model variables the value of area averaged e-folding time τ also is longer than S, implying that τ is generally not a sufficiently stringent estimate of the sampling interval required for accurate statistics.

3.9. *Bandwidths of Model Variables*

The final statistic considered is the bandwidth, a fundamental measure of the sampling frequency necessary for capturing essentially all the information in a time series. If at each grid point (i, j) the time series of hourly samples of a variable V is decomposed into Fourier harmonics

$$V(i, j, t) = \sum_f \left\{ A_f(i, j) \cos\left(\frac{ft}{2\pi}\right) + B_f(i, j) \sin\left(\frac{ft}{2\pi}\right) \right\}$$

of different frequency f, then the power accumulated up to frequency α is

$$\sigma_\alpha^2(i, j) = \sum_f^\alpha \{A_f(i, j)^2 + B_f(i, j)^2\}$$

and the bandwidth β is that frequency such that a large fraction γ of the total power is captured:

$$\sigma_\beta^2(i, j) \geq \gamma \sigma_T^2(i, j)$$

The corresponding bandwidth sampling interval is

$$s_\gamma = 1/(2\beta)$$

Land and global averages of s_γ for $\gamma = 0.95$ and $\gamma = 0.99$ are listed in Table 1. It can be seen that the maximum acceptable sampling interval S is always greater than or equal to s_{99}. This indicates that a certain amount of information, which is unnecessary for accurate estimation of the mean or variance of a model variable, is discarded. The discarded information may be relevant for the estimation of other statistical quantities, however.

4. Summary and Conclusions

The ECMWF model variables display a wide range of sensitivity to sampling frequency, as evidenced by several different statistics. There is general qualitative agreement among these measures: relatively short e-folding times τ tend to be associated with short acceptable sampling intervals S and bandwidth intervals s_{95} or s_{99} and with low p values (high intradiurnal variability). However, there may be substantial quantitative differences among these measures. For example, the sampling interval S necessary to yield reasonably accurate climate statistics is sometimes in closer agreement with the e-folding time τ than with the more fundamental measures s_{95}/s_{99} of an appropriate sampling interval. It therefore does not seem feasible to prescribe general guidelines for determining acceptable sampling intervals for accurate estimation of first- and second-moment statistics from criteria based on bandwidth intervals. However, storing snapshots of variables at bandwidth intervals s_{99} insures that essentially all the information present in the original time series is retained.

With the exception of convective processes, cloud properties, and the vertical motion field, sampling frequency is not of much concern for the ECMWF atmospheric variables because their intradiurnal variability is modest. For example, once-per-day sampling is sufficient to obtain reasonably accurate statistics of atmospheric specific humidity, temperature, and wind (although 18-hour rather than 24-hour sampling intervals are recommended to avoid aliasing of the diurnal cycle [cf. *Thuburn*, 1991]). Infrequent sampling is even more appropriate for subsurface soil temperature and moisture. Sampling is more problematical, however, for many of the surface fields because of their shorter time scales and larger intradiurnal variability. For these fields aliasing of the semidiurnal cycle and higher-frequency harmonics must be taken into account, and thus the ability to obtain more accurate statistics by sampling at the NID frequencies is an attractive, albeit logistically less convenient, contingency.

The wide range of sensitivity of the ECMWF model variables to sampling frequency makes it impractical to recommend an all-purpose storage strategy. First, for example, a choice must be made between storing variables as accumulations or as snapshots. Although accumulation allows exact calculation of model statistics, this is only practical if all quantities of interest can be identified a priori and computed efficiently during the simulation. On the other hand, retaining snapshots of model fields permits a posteriori calculation of the time series of additional derived variables. Thus saving snapshots of key model fields along with accumulations of selected variables is likely to be the preferred storage strategy for many climate applications.

If snapshots are stored at 6-hour intervals, the climate statistics of the majority of ECMWF model variables can be estimated with reasonable accuracy and the semidiurnal cycle also can be resolved. (Moreover, observational data for model validation usually are not available at more frequent intervals.) Nevertheless, a 6-hour storage interval does not permit accurate estimation of the first- and second-moment statistics of surface heat fluxes and atmospheric convective processes, nor does it adequately capture the high-frequency variability of accumulated precipitation and runoff.

Alternative strategies to 6 hourly storage therefore are worth considering. Ideally, it would be desirable to save snapshots (and accumulations of variables such as precipitation and runoff) at 3-hour intervals since this would allow sufficient sampling of the most rapidly fluctuating model variables and consistent calculation of derived quantities such as fluxes of momentum, moisture, and heat. If such a storage scheme is impractical, a reasonable compromise would be to save snapshots of only the most rapidly varying fields at 3-hour intervals or to save their accumulations every 6 hours. Where accurate estimation of the first-moment statistics of the surface variables is important for particular applications, storage at NID intervals may be recommended, but such a scheme should be adopted only after insuring the absence of systematic biases in the second-moment statistics. Finally, if storage constraints are so severe that a long model history can be saved only twice a day, it is better to store variables at 11-hour rather than 12-hour intervals in order to avoid errors associated with the aliasing of the semidiurnal cycle.

We caution that some results of this study may be model-specific, in that the characteristic time scales of simulated climate processes probably are influenced by the particular choices of physical/dynamical parameterizations. These results may also depend on horizontal and vertical resolution, the frequency of model physics calculations, and the perpetual July simulation. Our analysis therefore should be viewed as provisional information on the sampling problem, and we encourage similar investigations of other general circulation models.

Acknowledgments. The cooperation of the European Centre for Medium-Range Weather Forecasts in making their model available for this research is gratefully acknowledged. We also thank Ben Santer for helpful discussions on the sampling problem and John Thuburn for supplying a preprint of his study and for commenting on

an earlier version of this paper. This work was performed under the auspices of the U.S. Department of Energy, Environmental Sciences Division, by the Lawrence Livermore National Laboratory under contract W-7405-ENG-48.

REFERENCES

Alexander, R. C., and R. L. Mobley, Monthly average sea-surface temperatures and ice-pack limits on a 1 degree global grid, *Mon. Weather Rev.*, *104*, 143–148, 1976.

Boer, G. J., and M. Lazare, Some results concerning the effect of horizontal resolution and gravity-wave drag on simulated climate, *J. Clim.*, *1*, 789–806, 1988.

Boer, G. J., N. A. McFarlane, R. Laprise, J. D. Henderson, and J. P. Blanchet, The Canadian Climate Centre spectral atmospheric general circulation model, *Atmos. Ocean*, *22*, 397–429, 1984.

Boville, B. A., Sensitivity of simulated climate to model resolution, *J. Clim.*, *4*, 469–485, 1991.

European Centre for Medium-Range Weather Forecasts (ECMWF) Research Department, ECMWF forecast model, adiabatic part, 2nd ed., *Res. Manual 2*, Reading, England, 1988*a*.

ECMWF Research Department, ECMWF forecast model, physical parameterisation, 2nd ed., *Res. Manual 3*, Reading, England, 1988*b*.

Fisher, R. A., *Statistical Methods for Research Workers*, Oliver and Boyd, Edinburgh, Scotland, 1925.

Hansen, J., G. Russell, D. Rind, P. Stone, A. Lacis, S. Lebedeff, R. Reudy, and L. Travis, Efficient three-dimensional global models for climate studies: Models I and II, *Mon. Weather Rev.*, *111*, 609–662, 1983.

Kidson, J. W., and K. E. Trenberth, Effects of missing data on estimates of monthly mean general circulation statistics, *J. Clim.*, *1*, 1262–1275, 1988.

Kiehl, J. T., and D. L. Williamson, Dependence of cloud amount on horizontal resolution in the NCAR community climate model, *J. Geophys. Res.*, *96*, 10,955–10,980, 1991.

Manabe, S., J. Smagorinsky, J. L. Holloway, and H. M. Stone, Simulated climatology of a general circulation model with a hydrologic cycle, III, Effects of increased horizontal computational resolution, *Mon. Weather Rev.*, *98*, 175–212, 1970.

Miller, M. J., T. N. Palmer, and R. Swinbank, Parameterization and influence of a subgrid scale orography in general circulation and numerical weather prediction models, *Meteorol. Atmos. Phys.*, *40*, 84–109, 1989.

Morcrette, J.-J., Radiation and cloud radiative properties in the ECMWF operational weather forecast model, *ECMWF Tech. Memo. 165*, 26 pp., Eur. Cent. for Medium-Range Weather Forecasts, Reading, Eng., 1989.

Phillips, T. J., The impact of sampling errors on the perceived response of a climate model to a sea surface temperature anomaly, *Atmos. Ocean*, *25*, 177–196, 1987.

Slingo, A. (Ed.), Handbook of the Meteorological Office 11-layer atmospheric general circulation model, *Rep. DCTN 29*, Meteorol. Off., Bracknell, Eng., 1985.

Thuburn, J., Data sampling strategies for general circulation models, *Q. J. R. Meteorol. Soc.*, *117*, 385–398, 1991.

Tiedtke, M., A comprehensive mass flux scheme for cumulus parameterization in large-scale models, *Mon. Weather Rev.*, *117*, 1779–1800, 1989.

Tokioka, T., K. Yamazaki, I. Yagai, and A. Kitoh, A description of the Meteorological Research Institute atmospheric general circulation model (MRI GCM-I), *Tech. Rep.*, *MRI 13*, 249 pp., Meteorol. Res. Inst., Tsukuba, Japan, 1984.

Trenberth, K. E., Climate diagnostics from global analyses: Conservation of mass in ECMWF analyses, *J. Clim.*, *4*, 707–722, 1991.

Wellck, R. E., A. Kasahara, W. M. Washington, and G. D. Santo, Effect of horizontal resolution in a finite-difference model of the general circulation, *Mon. Weather Rev.*, *99*, 673–683, 1971.

K. Arpe, Max-Planck-Institut für Meteorologie, Bundesstrasse 55, D-2000, Hamburg 13, Germany.

T. J. Phillips and W. L. Gates, Program for Climate Model Diagnosis and Intercomparison, L-264, Lawrence Livermore National Laboratory, P.O. Box 808, Livermore, CA 94550.

(Received September 17, 1991;
revised August 10, 1992;
accepted August 25, 1992.)